

# 99%-fidelity ballistic quantum-state transfer through long uniform channels

T. J. G. Apollaro,<sup>1,2</sup> L. Banchi,<sup>3</sup> A. Cuccoli,<sup>4,5</sup> R. Vaia,<sup>6</sup> and P. Verrucchi<sup>6,4,5</sup>

<sup>1</sup>*Dipartimento di Fisica, Università della Calabria,  
Via P.Bucci, 87036 Arcavacata di Rende (CS), Italy*

<sup>2</sup>*INFN-Gruppo collegato di Cosenza, Via P.Bucci, 87036 Arcavacata di Rende (CS), Italy*

<sup>3</sup>*ISI Foundation, Via Alassio 11/c, I-10126 Torino (TO), Italy*

<sup>4</sup>*Dipartimento di Fisica, Università di Firenze, Via G. Sansone 1, I-50019 Sesto Fiorentino (FI), Italy*

<sup>5</sup>*INFN Sezione di Firenze, via G.Sansone 1, I-50019 Sesto Fiorentino (FI), Italy*

<sup>6</sup>*Istituto dei Sistemi Complessi, Consiglio Nazionale delle Ricerche,  
via Madonna del Piano 10, I-50019 Sesto Fiorentino (FI), Italy*

(Dated: June 21, 2018)

Quantum-state transfer with fidelity higher than 0.99 can be achieved in the ballistic regime of an arbitrarily long one-dimensional chain with uniform nearest-neighbor interaction, except for the two pairs of mirror symmetric extremal bonds, say  $x$  (first and last) and  $y$  (second and last-but-one). These have to be roughly tuned to suitable values  $x \sim 2N^{-1/3}$  and  $y \sim 2^{3/4}N^{-1/6}$ ,  $N$  being the chain length. The general framework can describe the end-to-end response in different models, such as fermion or boson hopping models and  $XX$  spin chains.

## I. INTRODUCTION

Transferring quantum states between distant registers is one of the basic tasks that a quantum computer based on qubits located on fixed positions has to accomplish. The general scheme where a quantum channel physically connects the sending and the receiving qubits naturally emerges from such requirement and a variety of proposals have been recently put forward for realizing quantum channels for state transmission by different physical solutions: phonon modes for trapped ions [1] or photon modes for superconducting qubits [2, 3], molecular lattices for vibrational excitons [4] or optical lattices for cold atoms [5–8], arrays of coupled quantum dots [9–12], and interacting  $S = \frac{1}{2}$  spins on a one-dimensional lattice, usually referred to as spin chains. In particular, proposals based on spin chains were first introduced in this context by Bose [13, 14] and have attracted much attention in the last decade, due to both the possibility of exploiting their natural dynamics for the transfer process, and the availability of analytical results that allow for a detailed description of their dynamics.

All of the above mentioned proposals are based on the idea that the state of the sender-qubit be transferred at large distance via a dynamical site-to-site hopping mechanism that we will here describe in terms of a general *hopping model*. Once a 2-dimensional Hilbert space, generated by  $|0\rangle$  and  $|1\rangle$ , is assigned to each site  $i = 1, \dots, N$  of a one-dimensional lattice, the hopping model is defined by the following Hamiltonian:

$$\mathcal{H} = \frac{1}{2} \sum_{i,j=1}^N A_{ij} |\underline{i}\rangle\langle\underline{j}|, \quad (1)$$

where  $|\underline{i}\rangle \equiv |0\rangle^{\otimes i-1}|1\rangle|0\rangle^{\otimes N-i}$  is a brief notation for single-excitation states, and the structure of the hopping-amplitude matrix  $\mathbf{A} = \{A_{ij}\}$  depends on the properties of the specific model. Despite being responsible of a possible long-distance transfer process, such mechanism can

be generated by a short-range interaction. Notice that Eq. (1) describes free bosons as well as free fermions and, as far as the latter are concerned, an exact mapping exists between the Hamiltonian (1) and that of the  $S = \frac{1}{2}$   $XY$  chain, where the matrix elements  $A_{ij}$  correspond to the exchange couplings. By the hopping model the basic transmission mechanisms can be studied and characterized: this, in turn, can also enlighten on the specific role of nonlinearity [15–17], noise [18] and dissipation [19, 20].

The quality of the channel, as far as the transfer process is concerned, essentially depends on the hopping amplitudes  $A_{ij}$ ; in particular, it has been proven that locally engineered hopping amplitudes can lead to perfect state transfer [21–27]. However, strategies based on a very detailed design of the internal couplings appear very demanding from a practical point of view [28].

Having in mind that experimental setups generally require the couplings to be as uniform as possible (see, e.g., Ref. [29]), different authors have proposed alternative strategies for obtaining high-quality state-transfer processes through mirror-symmetric channels with uniform bulk and just a few extremal couplings allowed to be varied [30–35]. Some of these alternative strategies are based on the idea of markedly weakening the coupling between the channel and the sender/receiver qubits, a solution that has been shown [30, 32, 36] to lead to a very high-quality state transfer. However, this scheme yields large transmission times and requires such a reduction of the extremal bonds that a severe limitation on the actual length of a functioning channel must be taken into account.

In general, the transmission quality of almost uniform channels is expected to deteriorate as the length of the channel is increased [13, 14, 34] due to dispersion, which is integral to uniformly distributed couplings. On the other hand, modeling a scalable quantum-state transfer process whose quality depends as little as possible on the physical length of the channel is an essential issue to address, especially if solid-state implementations and/or

experimental analysis are in order.

Therefore, we find ourselves squeezed between the seemingly incompatible requirements of avoiding too much a detailed design of the physical channel and yet getting a reasonably long channel characterized by a relatively convenient transfer time.

Our approach for solving this puzzle stems from the idea of exploiting, in an almost uniform channel, the ballistic state-transfer mechanism that allows perfect transmission of a wavepacket [33, 37, 38], in virtue of a perfectly coherent, non dispersive, dynamics. Perfect-transfer follows from the requirement that the normal modes correspond to equally spaced eigenfrequencies (or, loosely speaking, to a linear dispersion relation), so that a coherent mirrored reconstruction of all normal components occurs [39]. We infer that only the modes involved in the initial configuration of the overall system need satisfying the linearity condition [33] in order to get an effectively ballistic dynamics: systems realizing this condition can be dubbed ‘optimal state-transfer’ systems.

This idea has been first proposed and implemented [33, 40] in a scheme where we could only play with one parameter of the Hamiltonian, namely the value of the extremal bond  $x = A_{12} = A_{N-1,N}$ .

We have learned that the emergence of an optimal value for  $x$  follows from quite a complex interplay between two conflicting effects, namely the deformation of the eigenvalue spacings and the shrinking of the mode distribution, which are simultaneously driven by the value of  $x$ . In order to further improve our results, we understand that these effects must be handled independently, a goal that can be accomplished by introducing just one more parameter in the model, as shown in this paper. Notice that the introduction of a second parameter in the model should not be thought of as a way of moving towards the perfect-transfer scheme (which requires  $N/2$  parameters) but rather as a practical answer to the effective need of controlling two competing effects.

In Section II the state-transfer mechanism in the hopping model Eq. (1) is studied and the quantities that characterize the efficiency of the quantum channel in terms of the transition amplitudes are obtained. In Section III we describe the setup for implementing the two-parameter optimal-transfer scheme (with two adjacent modified bonds at the ends of the chain) and derive implicit analytical expressions for the frequencies and the matrix elements entering the transition amplitude. The behavior of the latter is thoroughly discussed in Section IV, where numerical results are reported together with the analytical derivation of the large- $N$  limit of the attainable optimal transmission fidelity. In Section V the dynamical behavior is shown to be ballistic, i.e., the information is carried by a wavepacket traveling at constant speed along the channel. Conclusions are drawn in Section VI. Some details of the calculations are reported in Appendix A.

## II. STATE TRANSFER IN THE HOPPING MODEL

Let us consider the Hamiltonian (1). In the case of nearest-neighbor interaction the matrix  $\mathbf{A}$  is tridiagonal and, for the chain to be connected, the off-diagonal elements cannot vanish. Without loss of generality [41] we assume  $\mathbf{A}$  to be real with  $A_{i,i+1} = A_{i+1,i} > 0$ . Introducing the orthogonal matrix  $\mathbf{U} = \{U_{ni}\}$  that diagonalizes the matrix  $A$ ,

$$\sum_{ij} U_{ni} A_{ij} U_{mj} = \lambda_n \delta_{nm} \equiv 2\omega_n \delta_{nm}, \quad (2)$$

and the one-excitation states

$$|\underline{n}\rangle = \sum_i U_{ni} |\dot{i}\rangle, \quad (3)$$

the Hamiltonian turns into the diagonal form

$$\mathcal{H} = \sum_{n=1}^N \omega_n |\underline{n}\rangle \langle \underline{n}|. \quad (4)$$

If  $\mathbf{A}$  is mirror-symmetric, i.e., it commutes with the *mirroring matrix*  $\mathbf{J} = \{J_{ij} = \delta_{N+1-i,j}\}$ , then also  $\mathbf{J}$  is diagonalized by  $\mathbf{U}$ ,

$$\sum_j J_{ij} U_{nj} = U_{n,N+1-i} = j_n U_{ni}, \quad (5)$$

and since  $\mathbf{J}^2 = 1$  the eigenvalues  $j_n$  are either 1 or  $-1$ . It is proven in Ref. [42] that if the eigenvalues  $\omega_n$  are cast in decreasing order then  $j_n = (-1)^{n+1} = -e^{i\pi n}$ ; in other words, the  $n^{\text{th}}$  eigenvector of  $\mathbf{A}$  is mirror-symmetric or -antisymmetric according to whether  $n$  is odd or even.

### A. Estimating state-transfer quality

The purpose of state transfer is to start with a product state  $|\underline{\psi}\rangle = |\psi\rangle|0\rangle^{\otimes N-1}$ , with a generic state

$$|\psi\rangle = \alpha|0\rangle + \beta|1\rangle \quad (6)$$

of the first qubit, and let it evolve with  $\mathcal{H}$  in such a way that at a given time  $t \simeq N$  the state of the last qubit is as close as possible to  $|\psi\rangle$ . Formally, the evolved overall state is  $\rho(t) = e^{-i\mathcal{H}t} |\underline{\psi}\rangle \langle \underline{\psi}| e^{i\mathcal{H}t}$  and the instantaneous state at site  $i$  is

$$\rho_i(t) = \text{Tr}_{\{1,\dots,i-1,i+1,\dots,N\}} \rho(t). \quad (7)$$

Defining  $|\underline{0}\rangle = |0\rangle^{\otimes N}$ , the evolved overall state obeys

$$e^{-i\mathcal{H}t} |\underline{\psi}\rangle = \alpha |\underline{0}\rangle + \beta \sum_i \langle \dot{i} | e^{-i\mathcal{H}t} | \underline{1} \rangle |\dot{i}\rangle, \quad (8)$$

so that

$$\rho_i(t) = \begin{bmatrix} 1 - |\beta|^2 |u_i(t)|^2 & \alpha \beta^* u_i^*(t) \\ \alpha^* \beta u_i(t) & |\beta|^2 |u_i(t)|^2 \end{bmatrix}, \quad (9)$$



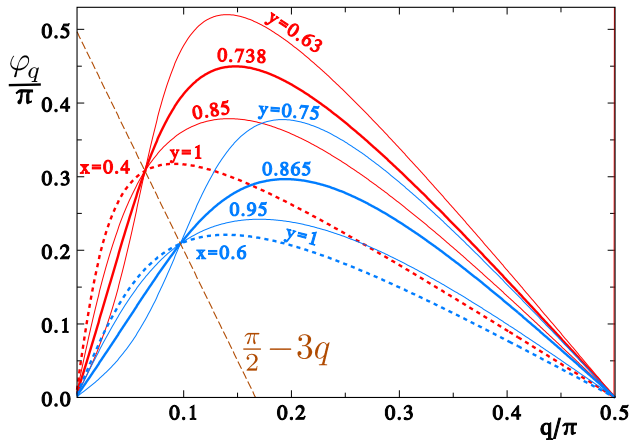


FIG. 2. (Color online) Shifts  $\varphi_q$ , Eq. (20), for different values of  $x$  and  $y$ . The dashed curves correspond to  $y=1$ . The fixed point  $q_F = \sin^{-1} \frac{x}{2}$  lies on the dashed straight line.

even  $N$  the  $m$ 's are half-integer: there is no qualitative difference between the outcomes for even and odd  $N$ , the latter case is just more easily handled numerically. The *phase shifts*

$$\varphi_q = \tan^{-1} \left[ \frac{y^2 \sin 2q}{x^2 - (2-y^2)(1 - \cos 2q)} \right] - 2q \quad (20)$$

displace the  $q$ -values from the equally spaced values of the fully uniform case ( $\varphi_q = 0$  for  $x=y=1$ ). Note that the phase shifts do not alter the sequence of the  $q_m$ 's, which increase with  $m$ .

Note that the denominator of Eq. (20) can vanish and the argument of  $\tan^{-1}$  can jump from  $\infty$  to  $-\infty$ , when this happens the conventional range of  $\tan^{-1}$  has to be extended above  $\pi/2$  rather than jumping from  $\pi/2$  to  $-\pi/2$ . In this way  $\varphi_q$  is a continuous function, shown in Fig. 2 for positive  $q$ . The effect of weakening the bond  $y$  is evident: the deformation is such that  $\varphi_q$  change its convexity in an interval  $|q| \lesssim q_F(x)$  whose width is characterized by the fixed point  $q_F(x) = \sin^{-1} \frac{x}{2}$ . Therefore, the parameter  $y$  can change the separation between the allowed  $q$ -values, and, in turn, between the eigenfrequencies affecting the coherence in the time evolution.

The mode distribution  $\mathcal{P}_k = U_{k1}^2$ , Eq. (A23), can be written in terms of  $q$  as

$$\mathcal{P}_q = \frac{2}{N+1+2\varphi'_q} \times \frac{x^2 y^2}{x^4 + (4-x^2-2y^2)^2 \tan^2 q - 16(1-y^2) \sin^2 q}. \quad (21)$$

The term in  $\varphi'_q$  is clearly irrelevant for a long chain, even though it ensures the normalization,  $\sum_m \mathcal{P}_{q_m} = 1$ , for any finite  $N$ . Fig. 3 describes the typical behavior of the mode density  $\mathcal{P}_q$  when  $y$  is varied keeping a fixed  $x < 1$ . Compared to its counterpart in the case of the uniform chain,  $x=y=1$ , it is evidently more structured; by lowering  $y$  its tails get increasingly suppressed and  $\mathcal{P}_q$  definitely changes to a bimodal shape with two symmetric

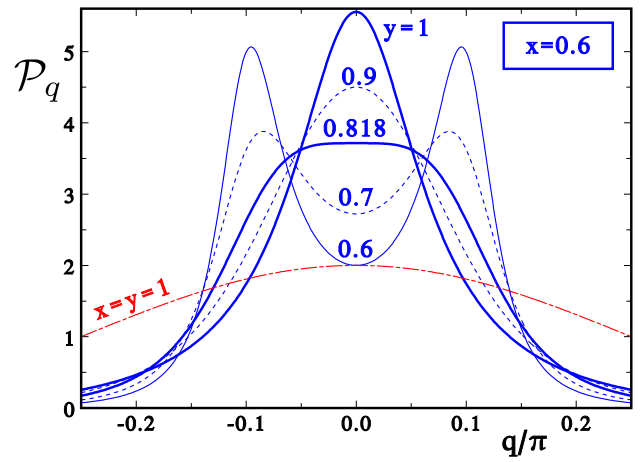


FIG. 3. (Color online) The normalized large- $N$  mode density  $\mathcal{P}_q$ , Eq. (21), for  $x=0.6$  and different values of the second bond coupling  $y$ . The thicker curves are those for  $y=1$  and for the threshold value  $y=Y(x)$  (see text and Fig. 4). The broad dash-dotted line is the result for the fully uniform chain,  $x=y=1$ .

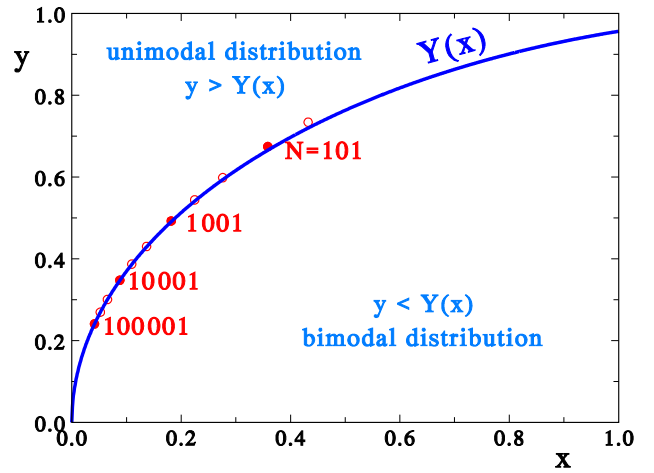


FIG. 4. (Color online) The function  $Y(x)$ , Eq. (22), separates the occurrence of unimodal and bimodal mode distributions. The optimized pairs  $(x, y)$ , i.e., those which maximize the arrival amplitude  $u(t)$ , are also reported for selected values of  $N$  (see Table I).

maxima: this occurs when in the denominator the coefficient of  $\sin^2 q$  becomes larger than that of  $\tan^2 q$ , i.e., when  $y$  is smaller than

$$Y(x) \equiv \sqrt{\sqrt{2}x - \frac{x^2}{2}}, \quad (22)$$

which is the curve shown in Fig. 4.  $\mathcal{P}_q$  is unimodal for  $y \geq Y(x)$  and has its maximum at  $q=0$ ; at the threshold  $y=Y(x)$  the maximum flattens, the deviation being  $\sim q^4$ , before developing the lateral maxima which are the more pronounced the smaller  $y$ . In the limit  $y \rightarrow 0$  the distribution  $\mathcal{P}_q$  tends to two symmetric  $\delta$ -peaks at  $q = \pm \sin^{-1} \frac{x}{2}$ , corresponding to the excitations of the single

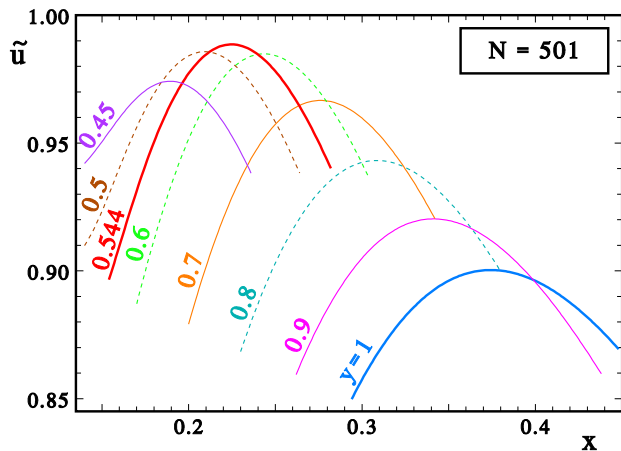


FIG. 5. (Color online) End-to-end amplitude at arrival  $\tilde{u}(x, y)$  as a function of  $x$  for selected values of  $y$  and  $N=501$ . The thicker curves correspond to  $y=1$  and to the optimized value  $y=0.5439$ .

dimer with interaction  $x$ , which is indeed isolated from the chain when  $y=0$ .

To represent the behavior of the level spacings, whose uniformity is crucial for the coherence of transmission, one can define a sort of ‘group velocity’ by

$$v_q \equiv \frac{N+1}{\pi} \omega'_q \partial_m q = \frac{N+1}{N+1+2\varphi'_q} \cos q, \quad (23)$$

where the ‘derivative’ of Eq. (19),  $(N+1+2\varphi'_q) \partial_m q = \pi$ , has been used, and from Eq. (20)

$$\varphi'_q = -2 + \frac{2y^2[x^2 + 2(2-x^2-y^2)\sin^2 q]}{x^4 + 4[y^4 - x^2(2-y^2)]\sin^2 q + 16(1-y^2)\sin^4 q}. \quad (24)$$

## IV. TRANSITION AMPLITUDE

### A. Numerical results

The transition amplitude between the sites 1 and  $N$  at the time  $t$  is given by Eq. (16). It can conveniently be rewritten as a sum over the allowed  $q$ ’s (19),

$$u(t) = \left| \sum_m \mathcal{P}_{q_m} e^{i(\pi m - t \sin q_m)} \right|. \quad (25)$$

This sum can be evaluated numerically: for any pair  $(x, y)$  our code solves iteratively the coupled Eqs. (19) and (20) and looks for the value of  $t \gtrsim N$ , i.e., the arrival time, where  $u(t)$  attains its largest value, say  $\tilde{u}(x, y)$ . Typical results for  $\tilde{u}(x, y)$  are reported as a function of  $x$  for selected values of  $y$  in Fig. 5, which refers to a chain of length  $N=501$ . One can see that taking  $y$  smaller than 1 the amplitude can become much closer to 1, also for the longest channels, and it is possible to identify the optimal values  $(x^{\text{opt}}, y^{\text{opt}})$  that make  $\tilde{u}(x, y)$  reach its maximum

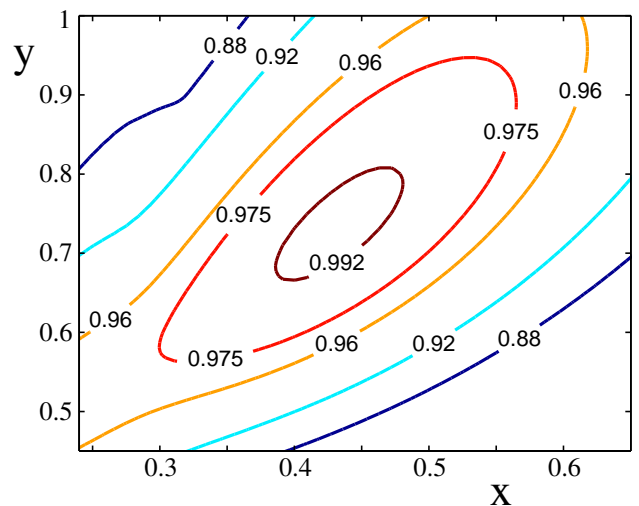


FIG. 6. (Color online) Contour plot of the average fidelity at arrival  $\mathcal{F}(x, y)$  in the  $(x, y)$  plane for  $N=51$ .

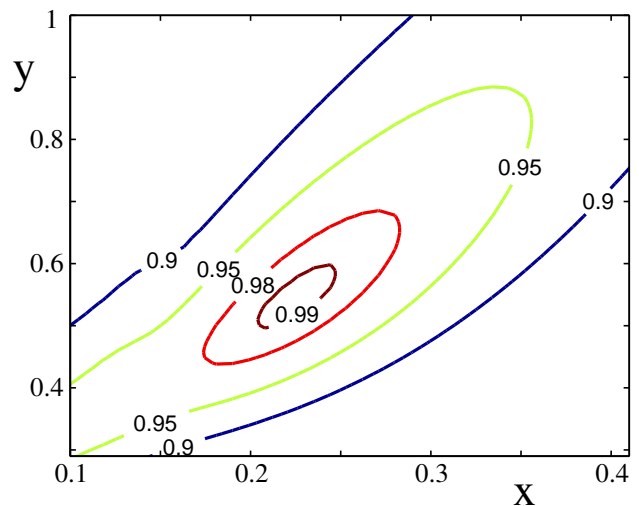


FIG. 7. (Color online) Contour plot of the average fidelity at arrival  $\mathcal{F}(x, y)$  in the  $(x, y)$  plane for  $N=501$ .

$u^{\text{opt}} \equiv \tilde{u}(x^{\text{opt}}, y^{\text{opt}})$ . Moreover, the maxima are so broad in the  $(x, y)$  plane that a relatively large mismatch from the optimal values still keeps giving a large amplitude, and consequently a large average transmission fidelity, as can be appreciated in the contour plots of Figs. 6 and 7.

The numerically evaluated optimal data are reported in Table I, together with those obtained in Ref. [40] by varying only  $x$  with  $y=1$ . Comparing with the latter, it is seen that the transfer quality improves in an extraordinary way: even for a chain of length  $N=50\,001$  the amplitude increases from 0.859 to 0.987, i.e., the state-transfer fidelity  $\mathcal{F}$  rises from 0.909 to 0.991. The values of Table I show that the optimized transmission amplitude decreases more and more weakly for large  $N$ , so that there could be a finite asymptotic amplitude attainable for an infinite chain: this is the case, indeed, as shown in the next subsection. In Fig. 8 the optimal values for

TABLE I. Optimal pairs  $(x^{\text{opt}}, y^{\text{opt}})$  and the corresponding amplitude  $u^{\text{opt}} = \tilde{u}(x^{\text{opt}}, y^{\text{opt}})$  and average fidelity  $\mathcal{F}^{\text{opt}}$  for different channel lengths  $N$ . Also reported are the optimal values obtained [40].

$N$	$x^{\text{opt}}$	$y^{\text{opt}}$	$u^{\text{opt}}$	$\mathcal{F}^{\text{opt}}$	$x^{\text{opt}}(y=1)$	$u^{\text{opt}}$	$\mathcal{F}^{\text{opt}}$
51	0.4322	0.7338	0.99270	0.99514	0.5542	0.9493	0.9666
101	0.3584	0.6742	0.99091	0.99395	0.4931	0.9324	0.9557
251	0.2760	0.5982	0.98932	0.99290	0.4216	0.9127	0.9431
501	0.2247	0.5439	0.98855	0.99239	0.3742	0.9003	0.9352
1 001	0.1818	0.4923	0.98849	0.99235	0.3322	0.8899	0.9286
2 501	0.1367	0.4300	0.98765	0.99179	0.2840	0.8791	0.9218
5 001	0.1097	0.3869	0.98747	0.99167	0.2523	0.8726	0.9178
10 001	0.0878	0.3474	0.98735	0.99159	0.2242	0.8674	0.9145
25 001	0.0652	0.3004	0.98726	0.99153	0.1920	0.8621	0.9112
50 001	0.05209	0.26925	0.98722	0.99151	0.1708	0.8590	0.9093
100 001	0.04150	0.24072	0.98720	0.99149	0.1519	0.8565	0.9078
$N \rightarrow \infty$	$1.954 N^{-1/3}$	$1.662 N^{-1/6}$	0.98715	0.99146	$1.030 N^{-1/6}$	0.8469	0.9018

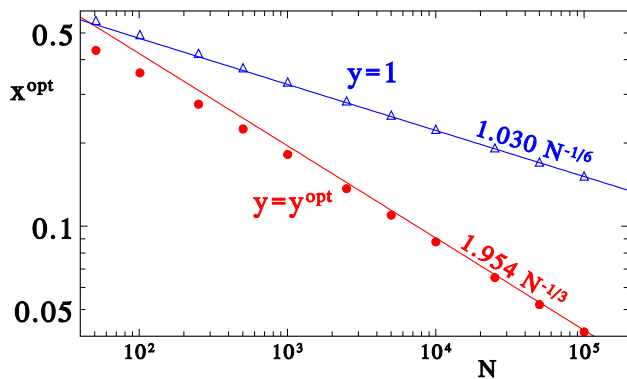


FIG. 8. (Color online) Optimal values for  $x$ , from Table I, reported vs.  $N$  both for  $y=1$  and for the optimized  $y=y^{\text{opt}}$ . Note that  $x \sim N^{-1/6}$  in the former case, while  $x \sim N^{-1/3}$  in the latter.

$x$  are reported for  $y=1$  and for  $y=y^{\text{opt}}$ . As shown formally in the next subsection, it turns out that  $x^{\text{opt}}$  scales as  $N^{-1/6}$  in the former case, while it obeys a new scaling law, apparently  $N^{-1/3}$ , in the latter.

The great improvement in transmission quality deals with the same argument we gave in Ref. [40]: although a constant group velocity  $v_q$  yields perfect transmission, it is sufficient that  $v_q$  be constant for the  $q$ -modes excited by the initialization of the first qubit whose distribution is  $\mathcal{P}_q$ . The results illustrated above confirm that the possibility of controlling, by means of *two* parameters ( $x$  and  $y$ ), the *two* most relevant features, shape of  $\mathcal{P}_q$  and stability of  $v_q$ , allows us to obtain an optimal trade-off leading to nearly perfect transmission.

The weaker second bond  $y$  acts indeed on the group velocity, as it appears in Fig. 9, where the shape of  $v_q$  is reported for the optimized value of  $x$ , and compared with the corresponding mode density  $\mathcal{P}_q$ . With a smaller

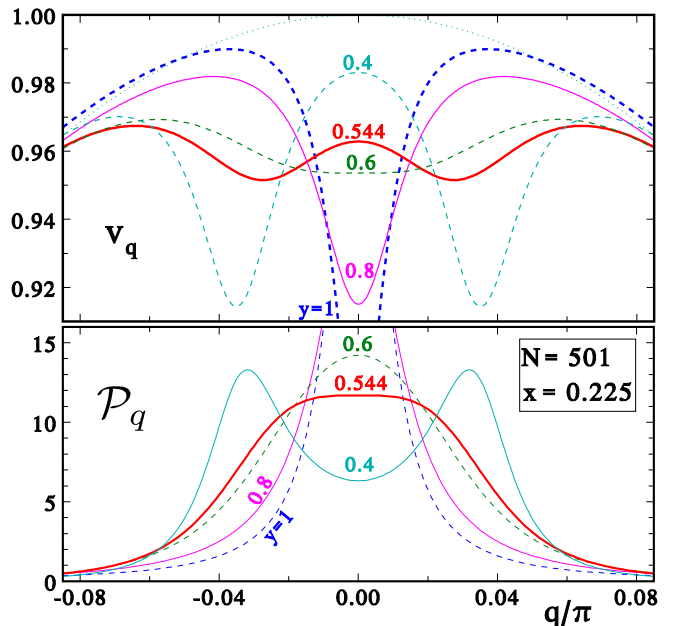


FIG. 9. (Color online) Group velocity  $v_q$  and corresponding mode density  $\mathcal{P}_q$  for  $N=501$ ,  $x=x^{\text{opt}}=0.225$ , and selected values of  $y$ . The thicker curves correspond to  $y=1$  (dotted) and to the optimized value  $y=y^{\text{opt}}=0.544$  (solid).

$y$ , the central dip appearing for  $y=1$  is strongly reduced and the group velocity just shows a small modulation in a rather wide range, so favoring a coherent dynamics; at the same time  $\mathcal{P}_q$  broadens, but not dramatically as it is mainly controlled by  $x$  (see, e.g., Fig. 4 of Ref. [40]); the optimized value  $y=y^{\text{opt}}$  clearly gives the best result compatible with the assumed parametrization.

## B. Asymptotic behavior for large $N$

The numerically estimated optimal pairs  $(x^{\text{opt}}, y^{\text{opt}})$  are shown in Fig. 4. They evidently lie almost exactly on the threshold curve  $Y(x)$  separating the unimodal from the doubly-peaked shape  $\mathcal{P}_q$ , i.e.,  $y^{\text{opt}} \simeq Y(x^{\text{opt}})$ . We expect this to hold in the large- $N$  regime, since the condition  $y = Y(x)$  clears the quadratic terms in the denominator of the density (21) leaving smaller tails  $\sim q^{-4}$ , thus allowing for a more effective cut of the modes involving the main nonlinear part of  $v_q$ . Therefore, instead of considering  $y$  as a free parameter, we fix it to be given by

$$y \equiv Y(x) = \sqrt{\sqrt{2}x - \frac{x^2}{2}} = 2^{1/4} x^{1/2} + O(x^{3/2}). \quad (26)$$

As  $N \rightarrow \infty$  the sum (25) can be written as an integral,

$$u_\infty(t) = \lim_{N \rightarrow \infty} \int dm \mathcal{P}_{q_m} e^{i(\pi m - t \sin q_m)}. \quad (27)$$

In order to evaluate this asymptotic expression, first note that from (19) one has to set  $\pi m = (N+1)q_m + 2\varphi_{q_m}$ , and  $\pi dm = (N+1+2\varphi'_q) dq$ , so that

$$u_\infty(t) = \lim_{N \rightarrow \infty} \int_{-\frac{\pi}{2}}^{\frac{\pi}{2}} \frac{dq}{\pi} \tilde{\mathcal{P}}_q e^{i[(N+1)q + 2\varphi_q - t \sin q]}, \quad (28)$$

where

$$\tilde{\mathcal{P}}_q = \frac{2x^2 y^2}{x^4 + (4-x^2-2y^2)^2 \tan^2 q - 16(1-y^2) \sin^2 q} \quad (29)$$

is exactly the normalized function reported in Fig. 3. As by increasing  $N$  the optimal distribution gets narrower and narrower, the denominator can be expanded taking into account the assumption (26):

$$\tilde{\mathcal{P}}_q \simeq \frac{2^{3/2} x^3}{x^4 + (2q)^4}; \quad (30)$$

hence, the width of the relevant  $q$ -region shrinks with  $x$ . Let us introduce the scaled variable  $\xi = 2q/x$ , which is of the order of unity, so that

$$\tilde{\mathcal{P}}_q dq \simeq \frac{\sqrt{2} d\xi}{1 + \xi^4}. \quad (31)$$

As for the phase in Eq. (28), the leading term of the expansion of Eq. (20) is

$$\varphi_q \simeq \tan^{-1} \frac{\sqrt{2} \xi}{1 - \xi^2}, \quad (32)$$

and, defining the arrival-time delay  $s$  by  $t \equiv N+1+s$ , the remaining terms read

$$(N+1)q - t \sin q = t(q - \sin q) - sq \simeq \tau \xi^3 - \sigma \xi, \quad (33)$$

where

$$\tau \equiv \frac{1}{6} \left(\frac{x}{2}\right)^3 t, \quad \sigma \equiv \frac{x}{2} s, \quad (34)$$

are the rescaled counterparts of the arrival time  $t \sim N$  and delay  $s \sim N^{1/3}$ . Eventually, the asymptotic value of the amplitude reads

$$u_\infty(\tau, \sigma) = \frac{\sqrt{2}}{\pi} \int_{-\infty}^{\infty} d\xi \frac{\exp[i(\tau \xi^3 - \sigma \xi + 2 \tan^{-1} \frac{\sqrt{2} \xi}{1 - \xi^2})]}{1 + \xi^4}. \quad (35)$$

For a numerical evaluation it is convenient to perform the substitution  $\xi = \tan z$ , and consider the maximization of

$$u_\infty = \frac{2\sqrt{2}}{\pi} \int_0^{\frac{\pi}{2}} dz \frac{1 + \tan^2 z}{1 + \tan^4 z} \cos \Phi(z), \quad (36)$$

with

$$\Phi(z; \tau, \sigma) = \tau \tan^3 z - \sigma \tan z + 2 \tan^{-1} \frac{\tan 2z}{\sqrt{2}}; \quad (37)$$

although this phase strongly oscillates for  $z$  close to  $\pi/2$ , the weighting function makes the numerical convergence easy. The overall maximum corresponds to  $(\tau, \sigma) = (0.15545, 3.1645)$ , and amounts to  $u_\infty = 0.987153$ , which is the asymptotic value reported in Table I together with the asymptotic scaling resulting from Eq. (34),

$$\begin{aligned} x^{\text{opt}} &\simeq 2 \left(\frac{6\tau}{N}\right)^{1/3} \simeq 1.954 N^{-1/3}, \\ y^{\text{opt}} &= Y(x^{\text{opt}}) \simeq 1.662 N^{-1/6}, \end{aligned} \quad (38)$$

while the delay scales as  $s = 2\sigma/x \simeq 3.239 N^{1/3}$ , so that the arrival time is

$$t \simeq N + 1 + 3.239 N^{1/3}. \quad (39)$$

## V. STATE-TRANSFER DYNAMICS

In Section II we introduced the instantaneous transition amplitude from site 1 to any site  $i$  of the chain, Eq. (10). This quantity substantially tells where the information concerning the initial quantum state sits at any time  $t$ . Indeed, it obeys the sum rule

$$\sum_i |u_i(t)|^2 = \sum_{n=1}^N U_{n1}^2 = 1, \quad (40)$$

so one can view the state-transfer process as the transmission of a traveling wavepacket of amplitude  $u_i(t)$  which is able to optimally rebuild most of its content in the single  $N$ -th site. Looking at the dynamics of this wavepacket sheds further light onto the ballistic transfer mechanism and allows for interesting comparisons, based on the data for  $|u_i(t)|$  reported in Figs. 10 and 11.

The first comparison is made in panels (a), (b) and (c) of Figs. 10 and 11, and involves: (a) the fully uniform channel, which displays a very dispersive dynamics and is indeed inefficient for transmission; (b) the channel

with only one optimized extremal bond [40], showing an increased coherence; (c) the further step with two optimized extremal couplings which improves transmission close to perfection. These features can be appreciated looking at the height of the arrival-time maxima in Fig. 10, and at the rugged features, more evident in Fig. 11, that represent the amplitude losses due to dispersion, according to Eq. (40). Fig. 11 makes also evident the increasing arrival delay from (a) to (b) and to (c), as a consequence of the slower packet injection and reconstruction due to the softened endpoint couplings.

Eventually, let us consider the case of perfect state transfer [23], which is obtained by designing all nearest-neighbor couplings along the chain proportionally to the height of a semicircle of radius  $N+1$  drawn over the chain,

$$A_{i,i+1} = A_{i+1,i} = \frac{\pi}{N+1} \sqrt{i(N-i)}; \quad (41)$$

the energy unit being arbitrary, it is chosen here such that the resulting linear spectrum

$$\omega_m = \frac{\pi}{N+1} m, \quad m = -\frac{N-1}{2}, \dots, \frac{N-1}{2}, \quad (42)$$

yields the exact arrival time  $t=N+1$ . Notice that, neglecting terms  $\sim N^{-1}$ , the maximum of the couplings  $\{J_i\}$  is  $\pi/2$ , their average is  $\pi^2/8$ , and their mean-square value is  $\pi/3$ ; this allows for a meaningful comparison with our model, and the corresponding data are reported in the panels (d) of Figs. 10 and 11. The modulated couplings determine a varying velocity of the wavepacket along the chain, at variance with its constant velocity in the uniform channel of panels (a-c).

## VI. CONCLUSIONS

We have shown that almost perfect ballistic quantum-state transfer with fidelity larger than 0.99 can be obtained in an unmodulated channel of arbitrary length  $N$ , just by allowing the two endpoint pairs of nearest-neighbor interactions,  $x$  and  $y$ , to assume optimal values ( $x^{\text{opt}}, y^{\text{opt}}$ ). In addition, this maximum of the transmission quality in the  $(x, y)$  plane, as measured by the average fidelity or equivalently by the transition amplitude (16), is so broad that an experimental realization would not be bound to a fine-tuning of the endpoint couplings, as Figs. 6 and 7 clearly show.

One might think that the approach presented here looks like the second step of a sequence that, by allowing further bonds to vary, would lead to perfect ballistic transmission as found in Ref. [23]. However, such deduction does not hold true: indeed, while the aim of Ref. [23] is that of obtaining perfect transfer by letting all normal modes to evolve coherently, here we look for high-quality transfer by requiring that only the modes excited by the initialization of the first qubit be able to evolve coherently. This is done within an effective scheme

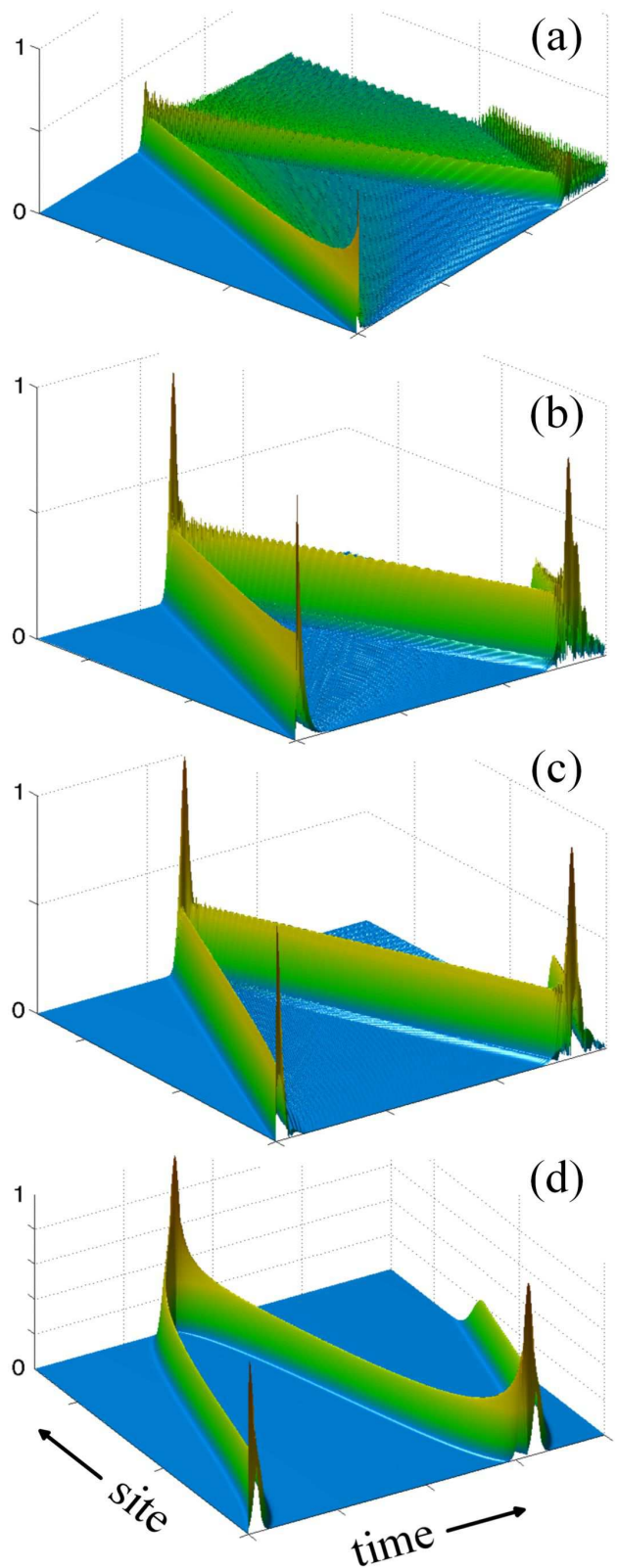


FIG. 10. (Color online) Space-time perspective views of the propagating wavepacket  $|u_i(t)|$ , Eq. (10), for a chain of length  $N=251$ , (a) in the fully uniform chain  $x=y=1$ , (b) in the case  $y=1$  and optimal  $x=0.422$  [40], (c) in the quasi-uniform channel, Eq. (17), with the optimal  $x=0.276$  and  $y=0.598$ , and (d) in the perfect-transfer channel [23], Eq. (41).



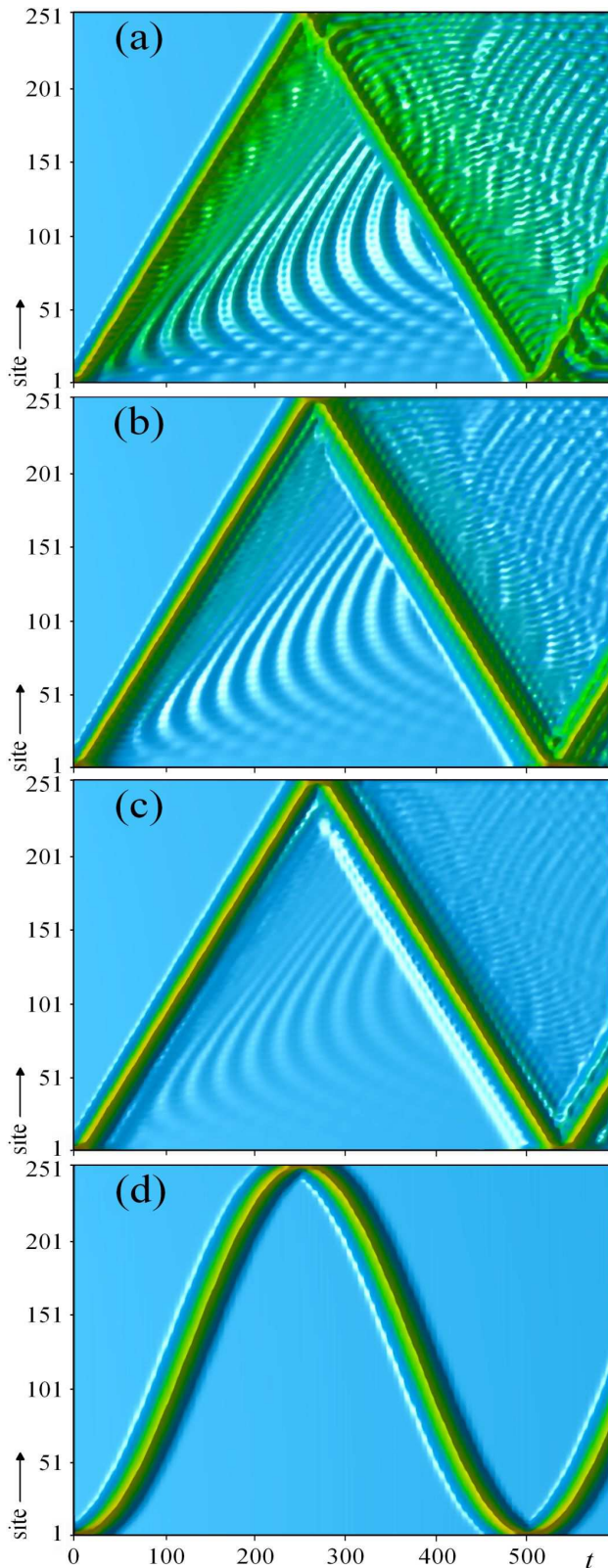


FIG. 11. (Color online) Space-time contour views of the propagating wavepacket  $|u_i(t)\rangle$ , Eq. (10) in the same cases of Fig. 10.

ruled by two effects, namely the mode distribution and the frequency spacings, that can be kept under control by just two parameters, i.e., the extremal couplings  $x$  and  $y$ . Our approach leads to extremal couplings  $x \sim N^{-1/3}$  and  $y \sim N^{-1/6}$ , sensibly larger than those required for perfect transfer, Eq. (41), which scale as  $N^{-1/2}$ .

The asymptotic results improve from the uniform chain ( $x = y = 1$ ) which gives fidelity  $\mathcal{F}_\infty = 1/2$ , to the single tuned bond [40] ( $y = 1$ ) giving  $\mathcal{F}_\infty = 0.902$ , and eventually to the optimal asymptotic fidelity evaluated in this paper,  $\mathcal{F}_\infty = 0.991$ . Whether comparable results could be obtained by other setups is difficult to say: the variants are numerous and we cannot tell a conclusive word in this respect.

The quasi-uniform channel here considered was previously used in Refs. [8, 43] for the different purpose of exploiting the quasi-long-distance entanglement shared by the extremal spins in the ground state in order to get efficient teleportation; in those papers, proposals for realizing the model by means of coupled cavity arrays and ultracold atoms in 1D optical lattices are put forward. We expect that such physical realizations might possibly fit also our setup. To this respect, we remark that when the presence of disorder in the couplings along the chain is taken into account, the one-parameter optimal state-transfer scheme ( $y = 1$ ) results to be more robust than the perfect-transfer one [18]; we expect such advantage to be preserved in the two-parameter optimal-transfer scheme.

We finally mention the similarity between the problem of quantum-state transfer and the subject of continuous-time quantum walks [44], where regular space-time structures called quantum carpets [45] can emerge from a complex dynamics: for instance, the revival of the wavefunction is analogous, in a mirror-symmetric context, to state transmission.

## ACKNOWLEDGMENTS

We acknowledge financial support from the Italian Ministry of University in the framework of the 2008 PRIN program (contract N. 2008PARRTS 003). TJGA is supported by the European Commission, the European Social Fund and the Region Calabria through the program POR Calabria FSE 2007-2013 - Asse IV Capitale Umano-Obiettivo Operativo M2. LB and PV gratefully thank Dr. A. Bayat and, with AC, Prof. S. Bose for useful discussions; TJGA thanks ISC-CNR for the kind hospitality.



with

$$v_k = 1 + (1-y^2)e^{-2ik} . \quad (\text{A17})$$

By deriving Eq. (A9) with respect to  $k$  one has

$$\begin{aligned} \sin k \partial_k \chi_N(k) &= \Im \left\{ e^{i(N+1)k} [i(N+1)u_k^2 + 2u_k u_k'] \right\} \\ &= (N+1) \Re \left\{ e^{i(N+1)k} u_k^2 \right\} + \\ &\quad + 2 \Im \left\{ e^{i(N+1)k} u_k u_k' \right\} ; \quad (\text{A18}) \end{aligned}$$

the argument of  $\Re$  is real by the secular equation so, using  $u_k'/u_k = \partial_k \ln u_k = \partial_k \ln |u_k| - i\varphi_k'$ ,

$$\begin{aligned} \sin k \partial_k \chi_N(k) &= \left[ N+1 + 2 \Im \left\{ \frac{u_k'}{u_k} \right\} \right] e^{i(N+1)k} u_k^2 \\ &= (N+1 - 2\varphi_k') e^{i(N+1)k} u_k^2 . \quad (\text{A19}) \end{aligned}$$

Eq. (A15) becomes

$$\begin{aligned} \mathcal{P}_k &= -\frac{2 \sin k}{N+1-2\varphi_k'} \frac{\Im \{ e^{iNk} u_k v_k \}}{e^{i(N+1)k} u_k^2} \\ &= \frac{2 \sin k}{N+1-2\varphi_k'} \frac{\Im \{ e^{ik} u_k v_k^* \}}{|u_k|^2} . \quad (\text{A20}) \end{aligned}$$

By means of Eqs. (A10) and (A17) one can express  $u_k = v_k(1+e^{-2ik}) - x^2 e^{-2ik}$ , and a simple expression of the numerator follows,  $\Im \{ e^{ik} u_k v_k^* \} = x^2 y^2 \sin k$ , finally yielding

$$\mathcal{P}_k = \frac{2x^2 y^2}{N+1-2\varphi_k'} \frac{\sin^2 k}{|u_k|^2} . \quad (\text{A21})$$

A manageable expression for  $|u_k|^2$  arises by working out Eq. (A10),

$$e^{2ik} u_k = -x^2 + 2(2-y^2) \cos^2 k + 2iy^2 \sin k \cos k , \quad (\text{A22})$$

and taking the square modulus, after some algebra the outcome is

$$\begin{aligned} \mathcal{P}_k &= \frac{2x^2 y^2}{N+1-2\varphi_k'} \times \\ &\quad \times \frac{1}{x^4 + (4-x^2-2y^2)^2 \cot^2 k - 16(1-y^2) \cos^2 k} . \quad (\text{A23}) \end{aligned}$$

An explicit expression for  $\varphi_k'$  can be found going back to Eq. (A19)

$$\varphi_k' = -\Im \left\{ \frac{u_k'}{u_k} \right\} = -\frac{\Im \{ u_k^* u_k' \}}{|u_k|^2} , \quad (\text{A24})$$

where, from Eq. (A10),

$$u_k' = -2i [u_k - 1 - (1-y^2)e^{-4ik}] , \quad (\text{A25})$$

and some further calculation gives

$$\begin{aligned} |u_k|^2 \varphi_k' &= 2 \Re \{ u_k^* [u_k - 1 - (1-y^2)e^{-4ik}] \} \\ &= 2|u_k|^2 - 2y^2 [x^2 + 2(2-x^2-y^2) \cos^2 k] . \quad (\text{A26}) \end{aligned}$$

Eventually, the mode density can be made fully explicit starting again from Eq. (A21),

$$\mathcal{P}_k = \frac{2x^2 y^2 \sin^2 k}{(N-3) \{ [x^2 - 2(2-y^2) \cos^2 k]^2 + 4y^4 \cos^2 k \sin^2 k \} + 4y^2 [x^2 + 2(2-x^2-y^2) \cos^2 k]} . \quad (\text{A27})$$

- 
- [1] J. I. Cirac and P. Zoller, Phys. Rev. Lett. **74**, 4091 (1995).  
[2] A. Blais, R.-S. Huang, A. Wallraff, S. M. Girvin, and R. J. Schoelkopf, Phys. Rev. A **69**, 062320 (2004).  
[3] C.-P. Yang, Phys. Rev. A **82**, 054303 (2010).  
[4] V. Pouthier, arXiv:1201.5184 (2012).  
[5] H.-J. Briegel, T. Calarco, D. Jaksch, J. I. Cirac, and P. Zoller, J. Mod. Opt. **47**, 415 (2000).  
[6] J. F. Sherson, C. Weitenberg, M. Endres, M. Cheneau, I. Bloch, S. Kuhr, Nature **467**, 68 (2010).  
[7] E. H. Lapasar, K. Kasamatsu, Y. Kondo, M. Nakahara, and T. Ohmi, J. Phys. Soc. Jap. **80**, 114003 (2011).  
[8] S. M. Giampaolo and F. Illuminati, New J. Phys. **12** 025019 (2010).  
[9] G. M. Nikolopoulos, D. Petrosyan, and P. Lambropoulos, J. Phys.: Condens. Matter **16**, 4991 (2004).  
[10] D. Petrosyan and P. Lambropoulos, Opt. Comm. **264**, 419 (2006).  
[11] S. Paganelli, G. L. Giorgi, and F. de Pasquale, Fortschr. Phys. **57**, 1094 (2009).  
[12] S. Yang, A. Bayat, and S. Bose, Phys. Rev. A **82**, 022336 (2010).  
[13] S. Bose, Phys. Rev. Lett. **91**, 207901 (2003).  
[14] S. Bose, Contemp. Phys. **48**, 13 (2007).  
[15] A. Bayat and S. Bose, Phys. Rev. A **81**, 012304 (2010).  
[16] A. Bayat, L. Banchi, S. Bose, and P. Verrucchi, Phys. Rev. A **83**, 062328 (2011).  
[17] L. Banchi, A. Bayat, P. Verrucchi, and S. Bose, Phys. Rev. Lett. **106**, 140501 (2011).  
[18] A. Zwick, G. A. Álvarez, J. Stolze, and O. Osenda, Phys. Rev. A **85**, 012318 (2012).  
[19] M. Rafiee, M. Soltani, H. Mohammadi, and H. Mokhtari, Eur. Phys. J. D **63**, 473 (2011).  
[20] M. L. Hu, Eur. Phys. J. D **64**, 531 (2011).  
[21] A. Kay, Int. J. Quant. Inf. **8**, 641 (2010).  
[22] P. Karbach and J. Stolze, Phys. Rev. A **72**, 030301 (2005).

- [23] M. Christandl, N. Datta, A. Ekert, and A. J. Landahl, Phys. Rev. Lett. **92**, 187902 (2004).
- [24] M.-H. Yung and S. Bose Phys. Rev. A **71**, 032310 (2005).
- [25] C. Di Franco, M. Paternostro, and M. S. Kim, Phys. Rev. Lett. **101**, 230502 (2008).
- [26] A. Zwick, G. A. Álvarez, J. Stolze, and O. Osenda, Phys. Rev. A **84**, 022311 (2011).
- [27] Y. Wang, F. Shuang, and H. Rabitz, Phys. Rev. A **84**, 012307 (2011).
- [28] P. Cappellaro, L. Viola, and C. Ramanathan Phys. Rev. A **83**, 032304 (2011).
- [29] C. Ramanathan, P. Cappellaro, L. Viola, and D. G. Cory, New J. Phys. **13** 103015 (2011).
- [30] A. Wójcik, T. Luczak, P. Kurzyński, A. Grudka, T. Gdala, and M. Bednarska, Phys. Rev. A **72**, 034303 (2005).
- [31] T. J. G. Apollaro and F. Plastina, Phys. Rev. A **74**, 062316 (2006).
- [32] L. Campos Venuti, C. Degli Esposti Boschi, and M. Roncaglia, Phys. Rev. Lett. **99**, 060401 (2007).
- [33] L. Banchi, T. J. G. Apollaro, A. Cuccoli, R. Vaia, and P. Verrucchi, Phys. Rev. A **82**, 052321 (2010).
- [34] E. B. Fel'dman, E. I. Kuznetsova, and A. I. Zenchuk, Phys. Rev. A **82**, 022332 (2010).
- [35] A. Zwick and O. Osenda, J. Phys. A **44**, 105302 (2011).
- [36] N. Y. Yao, L. Jiang, A. V. Gorshkov, Z.-X. Gong, A. Zhai, L.-M. Duan, and M. D. Lukin, Phys. Rev. Lett. **106**, 040505 (2011).
- [37] T. J. Osborne and N. Linden, Phys. Rev. A **69**, 052315 (2004).
- [38] H. Yadsan-Appleby and T. J. Osborne, Phys. Rev. A **85**, 012310 (2012).
- [39] D. L. Aronstein and C. R. Stroud, Phys. Rev. A **55**, 4526 (1997).
- [40] L. Banchi, T. J. G. Apollaro, A. Cuccoli, R. Vaia, and P. Verrucchi, New J. Phys. **13**, 123006 (2011).
- [41] B. N. Parlett, *The Symmetric Eigenvalue Problem* (SIAM, Philadelphia, 1998).
- [42] A. Cantoni and P. Butler, Linear Algebra Appl. **13**, 275 (1976).
- [43] S. M. Giampaolo and F. Illuminati, Phys. Rev. A **80** 050301 (2009).
- [44] O. Mülken and A. Blumen, Phys. Rev. E **71**, 036128 (2005).
- [45] W. Kinzel, Phys. Bl. **51**, 1190 (1995).
- [46] E. Lieb, T. Schultz, and D. Mattis, Ann. Phys. **16**, 407 (1961).